THE ASTROPHYSICAL JOURNAL, 523:585–592, 1999 October 1

EVOLUTION OF THE LIGHT ECHO OF SN 1991T[1]

W. B. SPARKS,[2] F. MACCHETTO,[3] N. PANAGIA,[3] AND F. R. BOFFI
Space Telescope Science Institute, 3700 San Martin Drive, Baltimore, MD 21218
D. BRANCH
Department of Physics and Astronomy, University of Oklahoma, Norman, OK 73019
M. L. HAZEN
Harvard-Smithsonian Center for Astrophysics, 60 Garden Street, Cambridge, MA 02138
AND
M. DELLA VALLE
Dipartimento di Astronomia, Università di Padova, Vicolo Osservatorio 5, 35122-Padova, Italy
Received 1999 February 16; accepted 1999 May 13

ABSTRACT

Schmidt et al. presented strong evidence (photometry and spectroscopy) that the late time optical emission of SN 1991T in the Virgo spiral NGC 4527 is caused by a light echo. Here, we present photometry with the Wide Field and Planetary Camera 2 and high-resolution imaging polarimetry and photometry with the Faint Object Camera on board the *Hubble Space Telescope*, which demonstrates that the feature is indeed a light echo of the original supernova. We show that the emission is spatially resolved, complex, and both growing in size and changing in morphology. The echo is slowly fading. Our primary interest is to use the echo for estimating the distance to the host galaxy geometrically (see 1994 work by Sparks). Given that the elapsed time since the supernova exploded is small and that the galaxy is relatively distant, the expected region of maximally polarized emission cannot be fully resolved as yet. However, we do find polarized emission at the center of the echo, and simple models may be used to yield a distance estimate. The models favor smaller distances, with ≈ 15 Mpc being the upper allowable distance, subject to caveats described in the text. The echo is consistent with being caused by a dust cloud of uniform density $n \sim 0.9$ cm^{-3} and extending to ≈ 50 pc in front of the supernova. It is encouraging that even in a case very far from ideal, we can use this type of observation to derive a distance.

Subject headings: galaxies: individual (NGC 4527) — galaxies: photometry — supernovae: individual (SN 1991T)

1. INTRODUCTION

A perennial problem in astronomy and astrophysics is the determination of distances. The usual means by which this is tackled is via the astronomical distance scale "ladder." Distances to the nearest astronomical objects are determined directly through parallax measurements, and beyond that, intrinsic luminosities are inferred and compared with measured fluxes, which leads to an estimate of the distance. Systematic errors compound as steps are taken up the ladder from common, faint nearby standards to more luminous, rarer standards that are useful to extragalactic distances.

Clearly, if this ladder can be circumvented and distances to extragalactic scales determined directly, then several desirable consequences would follow. We would obtain completely independent validation (or otherwise) of the calibration of the multitude of luminosity indicators in use and, hence, of the true distance scale. We would test the physical basis of the luminosity calibration where it exists, such as in Cepheids or novae, and the corrections for dependencies on metallicity and reddening.

Sparks (1994, 1996) proposed a method that has the potential, in principle, to achieve this goal. Simply, the surface of a supernova light echo is a paraboloid figure with the supernova at the focus, and the observer is looking "into" the paraboloid. The radius from the center of the event as projected onto the sky is equivalent to mapping out the scattering angle, from 180° at the center, to smaller scattering angles at larger radii. At a metric radius of ct (t the time since the supernova), the scattering angle is 90°; a well-known property of scattering is that the degree of polarization of the scattered light maximizes at that angle. Hence, if an image of polarization degree of the reflection nebula (or "light echo") is obtained, a ring should be visible corresponding to maximum polarization at 90° scattering. Since the metric diameter of the ring is known, $2ct$, the distance of the echo and, hence, of the host galaxy can be derived immediately from the ring's angular diameter. *No intermediate steps or calibrations are needed.*

Other geometric distance estimation methods are coming into play, including gravitational lensing of background variable quasars and maser sources around nuclear black holes. The lensing method is dependent on the model potential (Blandford and Narayan 1999) and has a utility confined to special configurations. The maser technique is also confined to a very few special cases (Miyoshi et al. 1995; Greenhill et al. 1995). Light echoes, by contrast, *could* be of wide utility since all galaxies have supernovae and most have at least some cool interstellar material.

There has been no systematic, sensitive search for late time light echoes from supernovae; hence, there is currently no way of knowing how common, or otherwise, the occurrence of useful echoes is. Boffi, Sparks, & Macchetto

[1] Based on observations with the NASA/ESA *Hubble Space Telescope*, which is operated by AURA, Inc., under NASA contract NAS 5-26555 and by STScI grant GO-06713.01-95A.

[2] Visiting Scholar, The Johns Hopkins University, on sabbatical leave from Space Telescope Science Institute; sparks@stsci.edu.

[3] Affiliated with the Astrophysics Division of the European Space Agency, ESTEC, Noordwijk, Netherlands.

(1999) present the first effort to survey in a general way the sites of a large number of historical supernovae with that aim in mind. They identify supernova light echo candidates in about 25% of the 64 sites observed; however, additional observations are required before the true nature of these features can be established.

Meanwhile, there is the interesting case of SN 1991T, which occurred in NGC 4527, a spiral galaxy in the direction of the Virgo Cluster with a velocity of 1738 km s^{-1} (Sandage & Tammann 1987). This supernova was unusual in a number of ways for a Type Ia supernova, given that it showed abnormally weak spectral features premaximum and an unusually luminous broad maximum. At late times, the characteristic exponential fading of the supernova ceased. Schmidt et al. (1994) presented strong evidence that the late time emission is a light echo. Its luminosity essentially ceased to decline, and its very blue spectrum was shown to be consistent with a scattered (higher scattering efficiency in the blue), time-integrated spectrum of the supernova around its maximum. They concluded correctly, as we show in this paper, that the late time emission is a light echo.

This makes SN 1991T one of a very small number of known echoes—the others being around SN 1987A (Crotts 1988), Nova Persei (Kapteyn 1901), and possibly Nova Sagittarii 1936 (Swope 1940)—hence, we are interested in following its evolution and observing its properties in the context of gaining a deeper understanding of the likely utility of the echo method of geometric distance determination. Unfortunately, the rather recent explosion, and the distance of the host galaxy NGC 4527 (probably in the range 13–16 Mpc [Tully 1988; Fisher et al. 1999]), mean that we do not expect to resolve the maximum of polarization and make a direct measurement. We do attempt, below, to compare simple models with the data, however, and thus derive a distance by that route. Also, while SN 1991T was a peculiar supernova, it is unclear whether those peculiarities are related to the present-day echo, either directly through reprocessing of the supernova emission or indirectly through its location in a relatively dense environment. For a recent discussion of the spectrum and nature of SN 1991T, see Fisher et al. (1999).

Here, we present observations made with the *Hubble Space Telescope* (*HST*), using the Wide Field and Planetary Camera 2 (WFPC2) and Faint Object Camera (FOC), of the SN 1991T light echo. The WFPC2 images are continuum and line-emission images, while the FOC observations are imaging polarimetry in the blue at three separate epochs. We show that the feature is indeed a light echo and that it is evolving. We show that polarized emission is present and that, with models, a distance can be derived.

2. OBSERVATIONS

2.1. *Observational Material*

Table 1 gives the details of the observations discussed in this paper. To locate precisely and identify the optical counterpart of SN 1991T securely, two precursor observations were made with WFPC2 prior to the high-resolution imaging polarimetry with the FOC. In a single orbit, two observations with each of the F606W (*R*) and F658N (Hα + [N II] at the host redshift) filters were made. Figure 1 shows the broadband F606W WFPC2 image. (At the location of SN 1991T, the narrowband image is blank. The corresponding flux upper limit is presented below.)

Subsequently, a series of FOC observations were made using the F342W filter centered at $\approx$340 nm in conjunction with the three polarizing elements of the FOC. The instrument and these filters are described in detail in Nota et al. (1996). The FOC offers the highest spatial resolution imaging on *HST*, with a pixel size of 14 mas, and has a robust imaging polarization capability. The polarizers are three high-quality double Rochon prisms, oriented at 60° to one another, that provide essentially perfect polarization characteristics. Images are taken of the target with each of the polarizers in turn, accompanied by a fixed wavelength filter. We used the F342W filter, which is approximately at the peak of the FOC detector response. Figure 2 shows the 512 × 512 FOC field of view for the first epoch, presenting the three polarization images summed together. Figure 3 shows the images of the SN 1991T light echo alone, for each epoch of observation summed together, in order to show the time evolution of the echo.

Figure 4 shows images of the echo through each of the polarizers in turn for the 1998 May observations. Clear differences between these images reveal the presence of polarized light, which we study in greater detail below.

2.2. *Photometry*

The total flux of the echo was measured using standard calibration procedures for *HST* observations (Voit 1997). All images were first registered spatially using flux-

TABLE 1

HST OBSERVATIONS OF THE SN 1991T LIGHT ECHO

Instrument	Spectral Element	Exposure[a] (s)	Date	Aperture
WFPC2.....	F658N	1400.0	1996 Dec 07	PC1
WFPC2.....	F606W	600.0	1996 Dec 07	PC1
FOC/96.....	POL0; F342W	2374.5	1996 Dec 22	512 × 1024
FOC/96.....	POL60; F342W	2487.5	1996 Dec 22	512 × 1024
FOC/96.....	POL120; F342W	2373.5	1996 Dec 22	512 × 1024
FOC/96.....	POL0; F342W	2375.75	1997 Dec 28	512 × 512
FOC/96.....	POL60; F342W	2548.75	1997 Dec 28	512 × 512
FOC/96.....	POL120; F342W	2374.75	1997 Dec 28	512 × 512
FOC/96.....	POL0; F342W	2375.5	1998 May 10	512 × 512
FOC/96.....	POL60; F342W	2548.5	1998 May 10	512 × 512
FOC/96.....	POL120; F342W	2374.5	1998 May 10	512 × 512

[a] All exposure times are the sum of two separate observations.

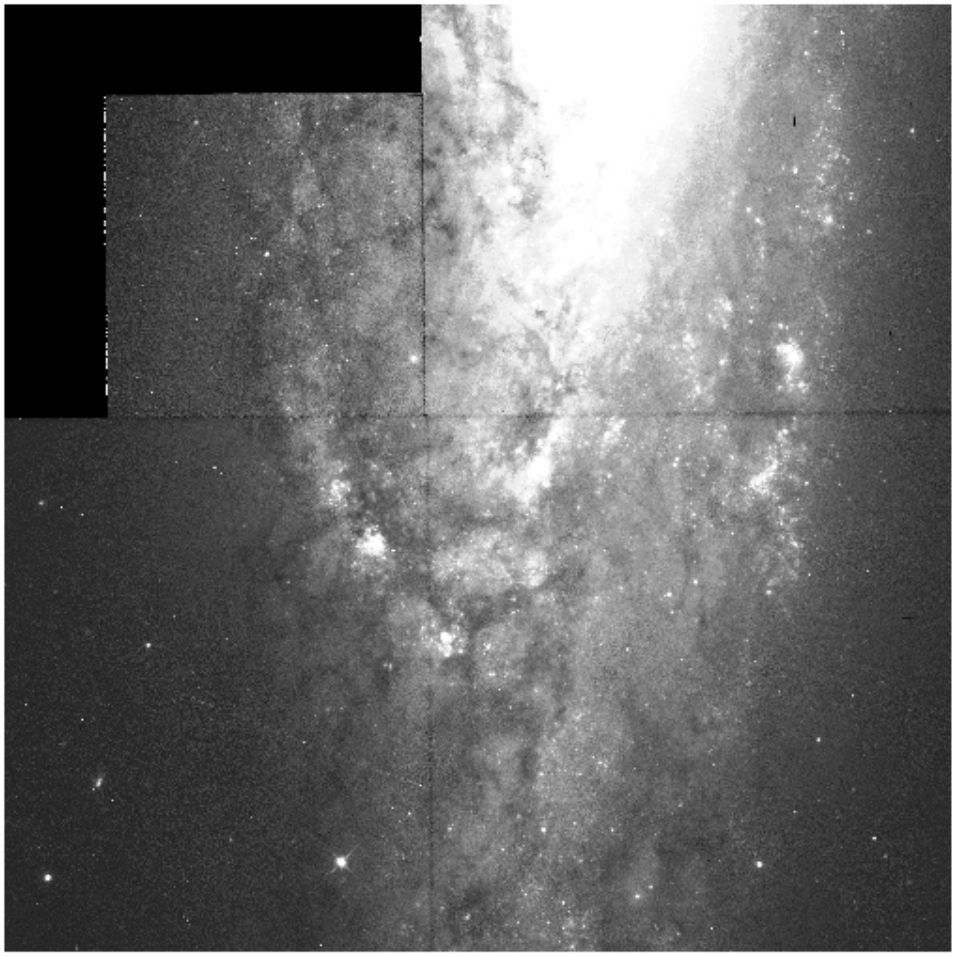

FIG. 1.—WFPC2 image of NGC 4527 with the SN 1991T light echo centered in the smaller PC field of view

conserving linear interpolation. Allowance was made for the format-dependence of FOC sensitivity. Background count rates, sky plus detector dark, were measured in regions avoiding the echo, and the total emission of the echo was inferred from the observed total count rate using the latest available absolute calibrations for both the WFCP2 and the FOC. The IRAF routine "radprof" was used to make the measurements for the FOC observations, while a simple rectangular region was used on the lower resolution WFPC2 data.

As a check, star 4 of Schmidt et al. (1994) is within the WFPC2 field of view. We measured its magnitude to be $M(\mathrm{F606W}) \approx 18.2$ relative to Vega, which, for a $V-I=2.0$ (Schmidt et al. 1994), implies $V \approx 18.7$ (Holtzman et al. 1995). This is consistent with the magnitude derived by Schmidt et al. (1994) of $V=18.63$, since the two brightest pixels of this star are saturated in the WFPC2 images.

The Hα + [N II] image yielded a flux of $(0.53 \pm 1.37) \times 10^{-18}$ ergs s^{-1} cm^{-2} Å^{-1}, which we present as a 3 σ upper limit in Table 2.

2.3. *Polarimetry*

The total flux of the echo for each of the three polarizers was compared to determine if there was measurable total polarization; this was done for each epoch. However, for each epoch, we derive a total integrated degree of polarization of approximately 0.04 ± 0.04, i.e., 4%, and there is no consistency in the derived position angles of polarization.

TABLE 2

PHOTOMETRY OF SN 1991T LIGHT ECHO

Instrument	Date	Wavelength (nm)	Flux (ergs s^{-1} cm^{-2} Å^{-1})	Magnitude
WFPC2.....	1996 Dec 7	600	4.7×10^{-18}	21.9 (V)
WFPC2.....	1996 Dec 7	658	$<4.1 \times 10^{-18}$ [a]	...
FOC1.....	1996 Dec 22	342	1.12×10^{-17}	21.16 (U)
FOC2.....	1997 Dec 28	342	1.03×10^{-17}	21.28 (U)
FOC3[b].....	1998 May 22	342	0.90×10^{-17}	21.46 (U)

[a] 3 σ upper limit.

[b] Central surface brightness $\approx 1 \times 10^{-16}$ ergs s^{-1} cm^{-2} Å^{-1} arcsec^{-2}.

FIG. 2.—FOC images of the SN 1991T 512 × 512 field of view for the first epoch of observation summed together. The light echo is the brightest feature slightly off center. The field is approximately 7″ on a side, and the *y*-axis position angle is −100°.

We conclude that there is no measurable integrated polarization to the accuracy we have. This is expected, since we show later in this paper that the polarization pattern is circularly symmetric and cancellation of the polarization of one part of the echo compared with another occurs when only the total flux is examined.

The signal-to-noise ratio (S/N) of the images is good enough to measure resolved polarized emission in the latest

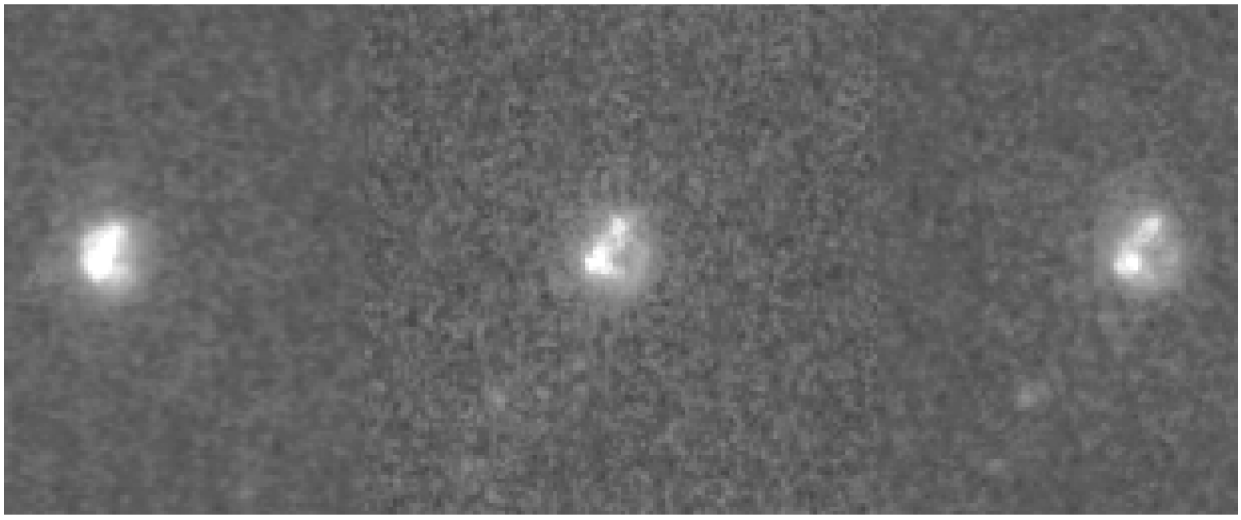

FIG. 3.—FOC images of the SN 1991T light echo at three separate epochs from 1996 December to 1998 May showing the feature becoming larger and more diffuse.

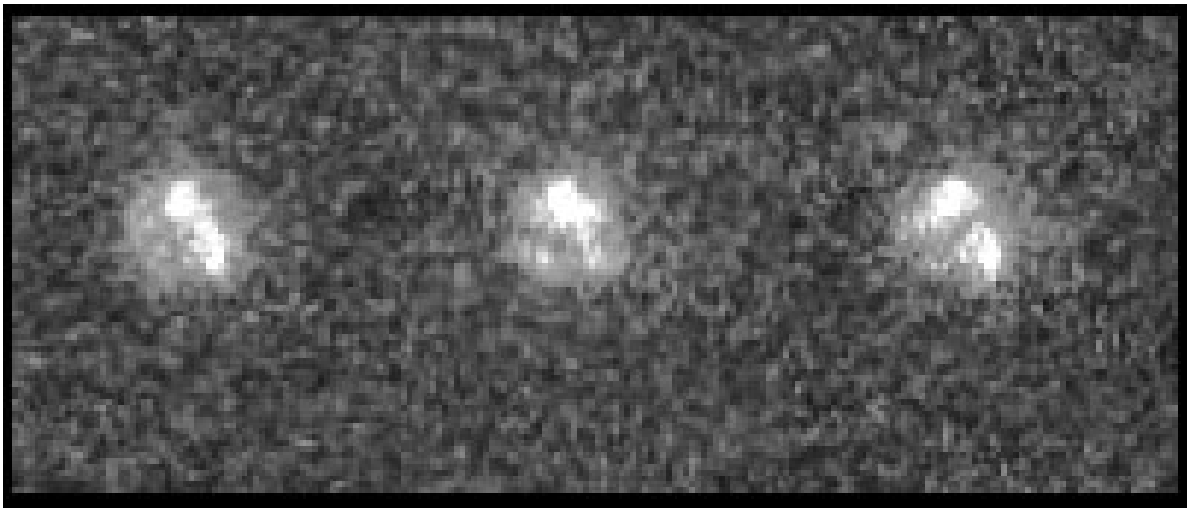

FIG. 4.—Images of the SN 1991T light echo taken with three different polarizers during 1998 May. *Left to right*: POL0, POL60, and POL120 filters, all in combination with the F342W filter.

data set from 1998 May. We derived polarization maps using a standard reduction procedure, which assumes that the three polarizers are perfectly efficient and oriented exactly at 60° to one another. We also assumed a Poisson noise distribution consistent with the flux levels observed in the image. To improve the S/N, the data were binned at 3 × 3 pixels. The analysis procedure employed is described in detail in Sparks & Axon (1999). In particular, we corrected for the positive-definite bias of polarization measurement using the mean value of the Rice distribution appropriate to the measured Stokes parameters (Serkowski 1958; Clarke & Stewart 1986; Sparks & Axon 1999).

Figure 5 shows polarization electric vectors overlaid on a contour map of the echo. The vectors show the circularly symmetric pattern expected for scattering caused by a single, central source. The center of the pattern of symmetry is within the echo complex. Polarization levels of up to ~30% are derived. At the center of the pattern, for radii less than 0.″05, the apparent polarization declines. This is expected, since, just as in the case of total integrated polarization, polarization with a roughly symmetric circular pattern cancels. We consider a specific model below.

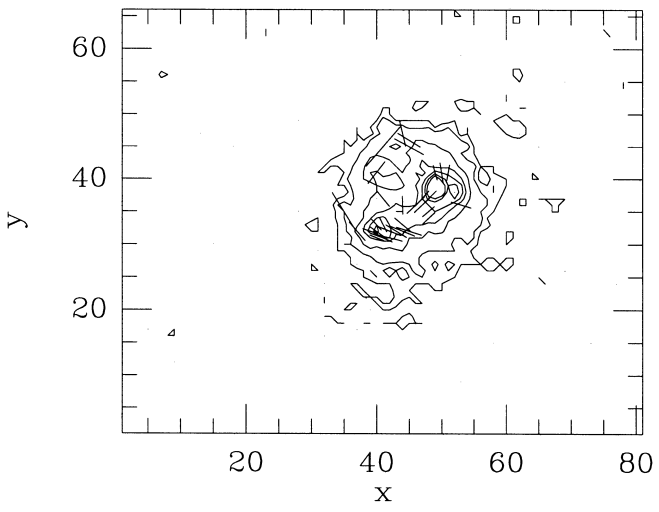

FIG. 5.—Polarization vectors superimposed on a contour map of the light echo of SN 1991T showing circular symmetry. Units of x and y are FOC pixels.

To determine the symmetry center more accurately, and to give better insight into the regularity of the polarization pattern, we generated an image of "caustics," which is shown in Figure 6. Here, for every pixel in the image, a straight line, or beam, is plotted perpendicular to the polarization vector appropriate to that pixel and with intensity proportional to the flux at that pixel. Essentially, all vectors can be seen to converge at a single point, which both defines the symmetry center of the polarization pattern to high accuracy and demonstrates the pure nature of the scattering pattern in this case. In the coordinate frame of Figure 5, the center of symmetry is at (44.4, 40.3).

3. DISCUSSION

To gain insight into the physical parameters required to produce an echo of this luminosity and size, we produced a set of model echoes based on a simple idealized case. Using a constant uniform density of $n = 1.0$ cm^{-3} (ignoring attenuation caused by foreground material) reaching to 50 pc in front of the supernova, for an initial supernova magnitude $U_{SN} = 11.3$ and distance of 15 Mpc, the echo flux declines from $U \approx 19.6$ to $U \approx 21.2$ from $T = 50$ days to $T = 2435$ days since the explosion. The expression for surface brightness is as in Sparks (1997), and the depth of 50 pc is based on an outer boundary of $r = 0.''2$. The actual observed echo flux is approximately 0.9 times this (see Table 2); hence, the implied interstellar density to produce an echo is of order $n \sim 0.9$ cm^{-3}. The implied column density to the supernova is 1.4×10^{20} cm^{-2} or an $E(B-V) \sim 0.02$. Careful examination of the WFPC2 image shows that the light echo is situated on the outer side of a spiral arm, the edge of which is defined by a prominent dust lane. The echo may very well be immersed within the dust lane (see Fig. 7). These quantities, therefore, seem reasonable given that the supernova appears to have exploded near the edge of a prominent dust lane.

Also, in this model we see a decline of about 10% between the first two FOC epochs, compared with an observed decline of ≈9%. Given the simplicity of the model, this

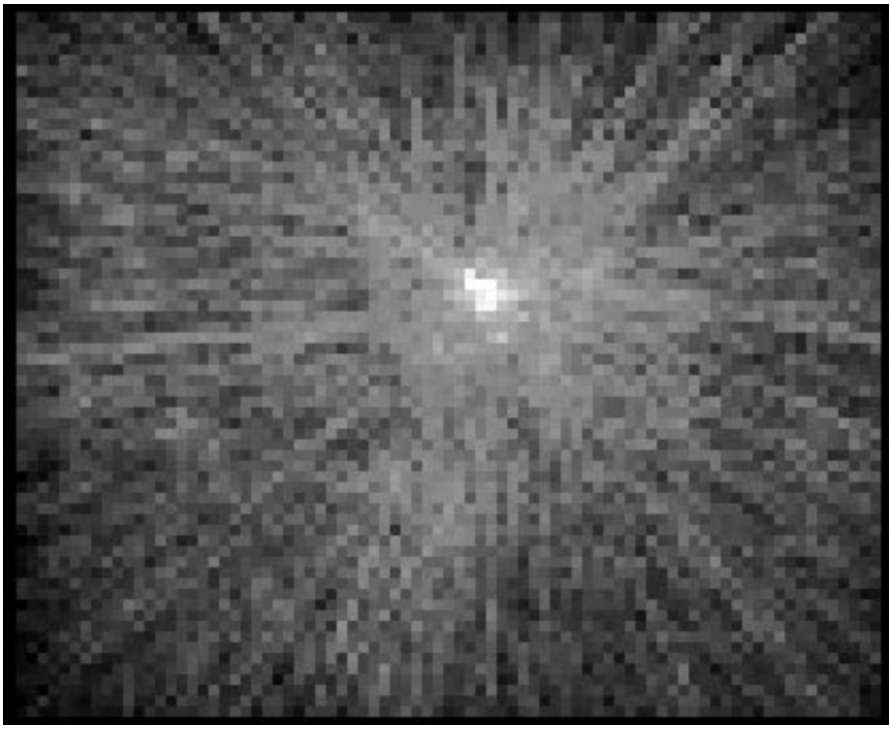

FIG. 6.—"Caustic" image of SN 1991T obtained by projecting vectors perpendicular to the polarization vectors, weighted by intensity, and showing a centrosymmetric scattering pattern with a well-defined center. The scattering center does not coincide with the intensity maxima.

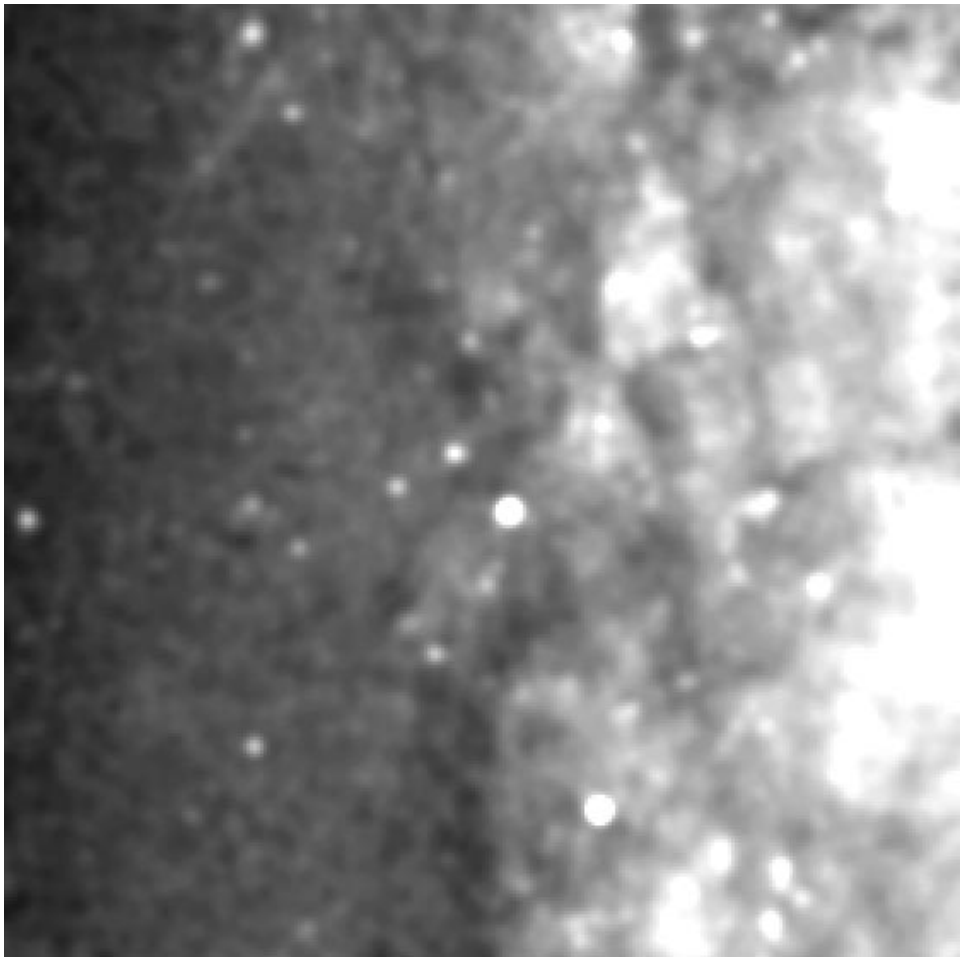

FIG. 7.—High-contrast, lightly smoothed WFPC2 image of the SN 1991T light echo showing complex regions of emission and dust absorption, with the echo at the center.

TABLE 3

EXPECTED RING DIAMETER OF THE SN 1991T LIGHT ECHO POLARIZATION MAXIMUM

Instrument	Date	Days since Maximum	$2ct$ (cm)	2ϕ[a] (arcsec)	2ϕ[b] (arcsec)
WFPC2.....	1996 Dec 7	2049	1.06×10^{19}	0.0355	0.0546
FOC1	1996 Dec 22	2064	1.07×10^{19}	0.0357	0.0550
FOC2	1997 Dec 28	2435	1.26×10^{19}	0.0421	0.0649
FOC3	1998 May 22	2568	1.33×10^{19}	0.0445	0.0684
ACS[c]	2002 Jul 1	4081	2.11×10^{19}	0.071	0.109

[a] Assuming a distance to NGC 4527 of 20 Mpc.
[b] Assuming a distance to NGC 4527 of 13 Mpc.
[c] Hypothetical observation with the Advanced Camera for Surveys, due to be installed on *HST* in 2000.

must be considered good agreement. The model change between the second and third epochs is insignificant, whereas we observe about a 5% decrease in apparent flux, which is comparable with the degree of instrumental uncertainty.

As may be seen from Table 3, the expected size of the ring of maximum polarization is small, essentially at the resolution limit of the FOC, which is $\sim$30 mas at 340 nm. Figure 8 shows the polarization degree that would be found for the case of the 1998 May epoch for a distance of 15 Mpc and a maximum degree of polarization of 1.0, both fully resolved and showing the effect of convolution with the FOC PSFs and 3×3 smoothing, as employed. The data are overlaid for comparison. The error bars shown are theoretically calculated $\pm 1\ \sigma$ errors for the data masked by S/N > 10 in total intensity. While there are departures from the model, in particular a secondary peak at 0.″16 radius, the levels of polarization found are similar to those of the model, and the initial rise and peak are approximately coincident. The secondary peak is only marginally significant, at 1–2 σ. Recall that 3×3 smoothing was used, while the sampling in the profile is by single pixel; hence, adjacent pixels are not strictly independent. (This was allowed for in the calculation of the error bars.) Overall, the observed and model profiles are in quite good agreement given the relatively low S/N of the data.

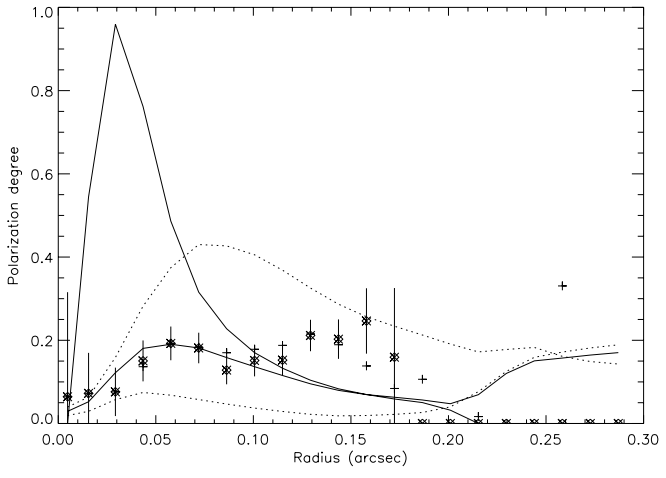

FIG. 8.—Azimuthally averaged polarization for SN 1991T light echo. The continuous lines show the uniform density model with a maximum degree of polarization of 1.0, for the cases of fully resolved and for FOC/PSF convolved with 3×3 pixel smoothing and a distance of 15 Mpc. The plus signs indicate all the data averaged, while the asterisks indicate data restricted to S/N > 10 in the output Stokes I image. The dotted lines illustrate the sensitivity to distance and show the same model at double and half the 15 Mpc distance.

To explore the allowed range of parameters further in the context of the uniform density model, we ran a set of equivalent simulations for distances running from 9 to 25 Mpc in steps of 2 Mpc and for maximum polarization degree running from 1.0 (100%) to 0.4 (40%). The derived profiles were then compared with the innermost 13 data points and a reduced χ^2 was calculated, $\chi^2 = (1/n) \sum_i [(d_i - m_i)/\sigma_i]^2$, where $d_i \pm \sigma_i$ are the data, $n = 13$, and m_i represents the model at each radius. The resulting χ^2 space is presented as the data in Table 4. Also, Figure 8 illustrates the sensitivity to distance by showing the 15 Mpc, $P_{\max} = 1.0$ model shifted to twice that distance and also to half that distance. As is apparent from the table and the plot, the models rapidly become unacceptable, and the distance is quite tightly constrained.

For the highest physically allowed values of intrinsic polarization, 100%, the allowed distances to SN 1991T are greatest. Distances in the range 13–15 Mpc give statistically acceptable solutions, with reduced $\chi^2 < 2$ (with 13 degrees of freedom, formally corresponding to a significance level of 0.02). In reality, we expect the maximum degree of polarization to be less than this. Models by White (1979) predict peak levels only around 30%; however, empirical measurements show significantly higher maximum degrees of polarization. If, for example, 60% is the maximum, then the allowed distance range is up to $\approx$12 Mpc in the uniform model. That is, as the peak polarization drops to lower values, the galaxy must be closer to provide the extended polarized emission we see. The maximum allowed distance in the context of this simple model is $\approx$15 Mpc. Cepheid

TABLE 4

REDUCED χ^2 VALUES FOR UNIFORM DENSITY ECHO MODELS

DISTANCE (Mpc)	$P_{\max}$ 1.0	0.8	0.6	0.4
9	8.86	3.56	1.28	1.99
11	3.29	1.59	1.65	3.48
13	1.78	1.73	2.78	4.91
15	1.9	2.6	4.02	6.13
17	2.63	3.66	5.17	7.12
19	3.55	4.69	6.16	7.91
21	4.48	5.63	7.	8.53
23	5.35	6.45	7.7	9.01
25	6.12	7.15	8.26	9.36

distances for two nearby galaxies, NGC 4496 and NGC 4536, yield distances of 16.4 ± 1.0 Mpc (Saha et al. 1996a, 1996b), while the catalog of Tully (1988) gives a distance of 13.0 Mpc for all three galaxies. If the galaxy is at the smaller distance, then the well-known "overluminosity" of SN 1991T would not be present.

The models developed suffer from several important uncertainties, since we are in the regime of an unresolved echo. In particular, we do not know (1) what the actual three-dimensional density distribution is, nor (2) whether there is any contaminating unpolarized light arising from sources other than the echo. In the case where an echo is well resolved, we expect these uncertainties to be much less of an issue. The latter will become apparent in due course as the echo fades away. Regarding the former, since the echo is apparently filled, it may not be as crucial as it might seem, since the degree of polarization should remain circularly symmetric, and we do not use intensity weighting in deriving the azimuthal average. If the echo under observation is resolved, the density distribution is not important, since it affects the *surface brightness* of the echo and not its polarization degree. Given these caveats, however, and our early stages of understanding of the optical properties of light echoes, we do not consider these distance estimates to be definitive.

Nevertheless, we are encouraged that, even in such a difficult case as SN 1991T, we obtain plausible distance estimates from rather straightforward models. For the first time, we are measuring symmetric, extended polarized emission in a distant light echo. These observations are very challenging, and significantly higher S/N will be required to develop substantially more constrained models in this particular case; but even with what we have, the χ^2 values constrain the distance to about a 10% uncertainty for any given set of model assumptions. Empirical measurement of the optical characteristics of dust scattering properties is highly desirable.

4. SUMMARY

We have shown conclusively that the optical emission from SN 1991T at the present time is caused by a light echo, thus confirming the analysis of Schmidt et al. (1994). We have presented well-resolved images of the emission, which is complex and $\approx 0\farcs4$ in diameter. We have shown that the echo is evolving in time and that it displays a symmetric scattering pattern of polarization vectors. The echo is fading by about 10% per year.

We have shown that simple, uniform density models can describe the general characteristics of the echo and can be used to estimate its distance even though the ring of maximum polarization is expected to be unresolved or only marginally resolved. The resulting distances are within the range of reasonable values from the literature, with a preference for the smaller values.

We cannot predict whether the echo will remain visible long enough to provide a simpler, direct geometric distance estimate to it as the ring expands and becomes fully resolved. That depends on the distribution of dust in the vicinity of SN 1991T. However, the presence of a strong light echo from SN 1991T shows that this phenomenon does occur, that it is potentially useful in distance estimation, and that additional efforts to locate older, bigger echoes would likely be worthwhile.

REFERENCES

Blandford, R. D., & Narayan, R. 1992, ARA&A, 30, 311
Boffi, F. R., Sparks, W. B., & Macchetto, F. 1999, A&A, in press
Clarke, D., & Stewart, B. G. 1986, Vistas Astron., 29, 27
Crotts, A. P. S. 1988, ApJ, 333, L51
Fisher, A., Branch, D., Hatano, K., & Baron, E. 1999, MNRAS, 304, 67
Greenhill, L. J., Jiang, D. R., Moran, J. M., Reid, M. J., Lo, K. Y., & Claussen, M. J. 1995, ApJ, 440, 619
Holtzman, J. A., Burrows, C. J., Casertano, S., Hester, J. J., Trauger, J., Watson, A. M., & Worthey, G. 1995, PASP, 107, 1065
Kapteyn, J. C. 1901, Astron. Nachr., 157, 201
Miyoshi, M., Moran, J., Herrnstein, J., Greenhill, L., Nakai, N., Diamond, P., & Inoue, M. 1995, Nature, 373, 127
Nota, A., Jedrzejewski, R., Voit, M., & Hack, W. 1996, Faint Object Camera Instrument Handbook, Version 7.0 (Baltimore: STScI)
Saha, A., Sandage, A., Labhardt, L., Tammann, G. A., Macchetto, F. D., & Panagia, N. 1996a, ApJ, 466, 55
———. 1996b, ApJS, 107, 693
Sandage, A. R., & Tammann, G. 1987, A Revised Shapley-Ames Catalog of Bright Galaxies (2d ed; Washington: Carnegie Institution)
Schmidt, B. P., Kirshner, R. P., Leibundgut, B., Wells, L. A., Porter, A. C., Ruiz-Lapuente, P., Challis, P., & Filippenko, A. 1994, ApJ, 434, L19
Serkowski, K. 1958, Acta Astron., 8, 135
Sparks, W. B. 1994, ApJ, 433, 29
———. 1996, ApJ, 470, 195
———. 1997, in STScI Symp. Ser. 10, The Extragalactic Distance Scale, ed. M. Livio, M. Donahue, & N. Panagia (New York: Cambridge Univ. Press), 281
Sparks, W. B., & Axon, D. J. 1999, PASP, 111, in press
Swope, H. H. 1940, Harvard Bull., 913, 11
Tully, R. B. 1988, Nearby Galaxies Catalogue (Cambridge: Cambridge Univ. Press)
Voit, M. 1997, *HST* Data Handbook (Baltimore: STScI)
White, R. L. 1979, ApJ, 229, 954